Climate
of the Past

Open Access

A 500-year seasonally resolved δ^{18}O and δ^{13}C, layer thickness and calcite aspect record from a speleothem deposited in the Han-sur-Lesse cave, Belgium

M. Van Rampelbergh[1], **S. Verheyden**[1,2], **M. Allan**[3], **Y. Quinif**[4], **H. Cheng**[5,6], **L. R. Edwards**[6], **E. Keppens**[1], and **P. Claeys**[1]

[1]Earth System Sciences, Vrije Universiteit Brussel (VUB), Pleinlaan, 1050 Brussels, Belgium
[2]Royal Belgian Institute of Natural Sciences, Geological Survey, Direction Earth and History of Life, Jennerstraat 13, 1000 Brussels, Belgium
[3]AGEs, Départment de Géologie, Université de Liège, Allée du 6 Août, B18 Sart-Tilman, 4000 Liège, Belgium
[4]Faculté Polytechnique, Université de Mons, Rue de Houdain 9, 7000 Mons, Belgium
[5]Institute of Global Environmental Change, Xi'an Jiaotong University, Xi'an 710049, China
[6]Department of Geological Sciences, University of Minnesota, 100 Union Street SE, Minneapolis MN 55455, USA

Correspondence to: P. Claeys (phclaeys@vub.ac.be)

Abstract. Speleothem δ^{18}O and δ^{13}C signals enable climate reconstructions at high resolution. However, scarce decadal and seasonally resolved speleothem records are often difficult to interpret in terms of climate due to the multitude of factors that affect the proxy signals. In this paper, a fast-growing (up to $2\,\text{mm}\,\text{yr}^{-1}$) seasonally laminated speleothem from the Han-sur-Lesse cave (Belgium) is analyzed for its δ^{18}O and δ^{13}C values, layer thickness and changes in calcite aspect. The studied record covers the period between AD 2001 and 1479 as indicated by layer counting and confirmed by 20 U / Th ages. The Proserpine proxies are seasonally biased and document drier (and colder) winters on multidecadal scales. Higher δ^{13}C signals reflect increased prior calcite precipitation (PCP) and lower soil activity during drier (and colder) winters. Thinner layers and darker calcite relate to slower growth and exist during drier (and colder) winter periods. Exceptionally dry (and cold) winter periods occur from 1565 to 1610, at 1730, from 1770 to 1800, from 1810 to 1860, and from 1880 to 1895 and correspond to exceptionally cold periods in historical and instrumental records as well as European winter temperature reconstructions. More relative climate variations, during which the four measured proxies vary independently and display lower amplitude variations, occur between 1479 and 1565, between

1610 and 1730, and between 1730 and 1770. The winters during the first and last periods are interpreted as relatively wetter (and warmer) and correspond to warmer periods in historical data and in winter temperature reconstructions in Europe. The winters in the period between 1610 and 1730 are interpreted as relatively drier (and cooler) and correspond to generally colder conditions in Europe. Interpretation of the seasonal variations in δ^{18}O and δ^{13}C signals differs from that on a decadal and multidecadal scale. Seasonal δ^{18}O variations reflect cave air temperature variations and suggest a 2.5 °C seasonality in cave air temperature during the two relatively wetter (and warmer) winter periods (1479–1565 and 1730–1770), which corresponds to the cave air temperature seasonality observed today. Between 1610 and 1730, the δ^{18}O values suggest a 1.5 °C seasonality in cave air temperature, indicating colder summer temperatures during this drier (and cooler) interval. The δ^{13}C seasonality is driven by PCP and suggests generally lower PCP seasonal effects between 1479 and 1810 compared to today. A short interval of increased PCP seasonality occurs between 1600 and 1660, and reflects increased PCP in summer due to decreased winter recharge.

1 Introduction

In the studied western European region, high-resolution climate records covering the last 500 years are scarce. Most climate information at seasonal or yearly scale is retrieved from historical data such as the price of flour or grapes (Van Engelen et al., 2001; Le Roy Ladurie, 2004), which may induce biases in the climate record. Therefore it is necessary to compare information from different archives, based on different approaches.

Speleothems have already often proven to enable climate reconstruction in Europe (Genty et al., 2003; Baker et al., 2011; McDermott et al., 2011; Fohlmeister et al., 2012; Verheyden et al., 2014). On millennial and centennial scales, the δ^{18}O and δ^{13}C variations can often be related to a single climate proxy such as temperature or vegetation cover (Spötl and Mangini, 2002; Genty et al., 2003; McDermott, 2005). However, on decadal and seasonal scale, a larger range of factors can influence the δ^{18}O, δ^{13}C, layer thickness or calcite aspect of a speleothem, making an interpretation in terms of climate more difficult. To allow reconstruction of the climate up to seasonal variation using mid-latitude speleothems, a detailed analysis of each used proxy must be compared with a multiproxy approach. Different European records have enabled climate to be successfully reconstructed through use of this approach (e.g., Frisia et al., 2003; Niggemann et al., 2003; Mangini et al., 2005; Mattey et al., 2008; Fohlmeister et al., 2012).

Belgian speleothems have the valuable advantage of often displaying a clear internal layered structure reflecting seasonal variations (Genty and Quinif, 1996). The link between layer thickness and water excess in Belgian stalagmites for the Late Glacial and Holocene period has clearly been demonstrated by Genty and Quinif (1996). The δ^{18}O and δ^{13}C signals from a speleothem sampled in the Père Noël cave were interpreted as being due to variations in cave humidity and drip rate inducing changes in the kinetics of the calcite deposition occurring closer or less close to isotopic equilibrium. More negative δ^{18}O and δ^{13}C values occur during periods of higher cave water recharge, when calcite deposition occurs closer to isotopic equilibrium (Verheyden et al., 2008). In this speleothem, the isotopic (δ^{18}O and δ^{13}C) and geochemical (Mg / Ca and Sr / Ca) proxies vary similarly and record the climate in terms of wetter and drier phases (Verheyden et al., 2014). The studied Proserpine stalagmite is a large tabularly shaped speleothem, growing in the Han-sur-Lesse cave, which is part of the same cave system as the Père Noël cave. A previous study of the stalagmite (Verheyden et al., 2006) revealed deposition from AD 200 to 2001, indicating an exceptionally high average growth rate of ± 1 mm yr^{-1}. The upper 56 cm, which covers the last 522 years is clearly layered. The similar variability in the δ^{18}O and δ^{13}C signals and the layer thickness was linked to changes in effective precipitation (rainfall minus evapotranspiration). These proxies therefore have the potential to be used to reconstruct climate in terms of wetter and drier phases.

In this paper we study this potential in more detail and up to a seasonally resolved timescale. An absolute age model is established by combining layer-counting ages with measured U / Th ages. A comparison of variations in layer thickness, calcite aspect, δ^{18}O and δ^{13}C signals in light of previous studies (Genty and Quinif, 1996; Verheyden, 2001; Genty et al., 2003; Mühlinghaus et al., 2007; Boch et al., 2009; Wackerbarth et al., 2010; Fohlmeister et al., 2012; Scholz et al., 2012; Verheyden et al., 2014) and monitoring of the same stalagmite location (Van Rampelbergh et al., 2014) leads to a better understanding of how these proxies are related and how they reflect climate variations. Comparing the Proserpine climate signal with winter temperature reconstructions in Europe (Le Roy Ladurie, 2004; Luterbacher et al., 2004; Dobrovolny et al., 2010) further verifies the proposed climate interpretation.

2 Study area

The Proserpine stalagmite is sampled in the Salle-du-Dôme chamber in the Han-sur-Lesse cave, southern Belgium (Fig. 1). The Han-sur-Lesse cave is a meander cutting of the Lesse river, which still flows through the cave. The large rooms, the multiple entrances and the presence of the river make it a well-ventilated cave. Part of the cave, including the Salle-du-Dôme, has been a show cave since the mid-19th century. The Salle-du-Dôme, which is the largest chamber of the cave system (150 m wide and 60 m high), is located under ca. 40 m of Givetian limestone (Quinif, 1988) with a C3-type vegetation-covered soil. The Proserpine stalagmite is a 2 m high stalagmite with a large tabular shape (70 cm large) that was actively growing when cored in 2001. A flow of seepage water throughout the year feeds the stalagmite. A property of such fast-growing "tam-tam-shaped" stalagmites is that they record climate signals and environmental information at high resolution (Perette, 2000).

The mean annual precipitation at the meteorological station of Han-sur-Lesse is 844 mm yr^{-1} and the mean annual air temperature averages 10.3 °C (Royal Meteorological Institute Belgium, hereafter RMI) characterizing a warm temperate, fully humid climate with cool summers (Kottek et al., 2006). While the temperature displays a well-marked seasonality with cool summers and mild winters, the rainfall is spread over the entire year. The external seasonality in temperature causes a subdued temperature variation within the Salle-du-Dôme of 2 to 2.5 °C between summer and winter (Van Rampelbergh et al., 2014). Present-day calcite is deposited in isotopic equilibrium with its drip water (Van Rampelbergh et al., 2014). The δ^{18}O signal of freshly formed calcite collected on top of the Proserpine stalagmite varies seasonally due the changes in cave air temperature. The δ^{13}C signal varies seasonally due to changes in prior calcite pre-

a) Han-sur-Lesse cave system   b) Proserpine stalagmite
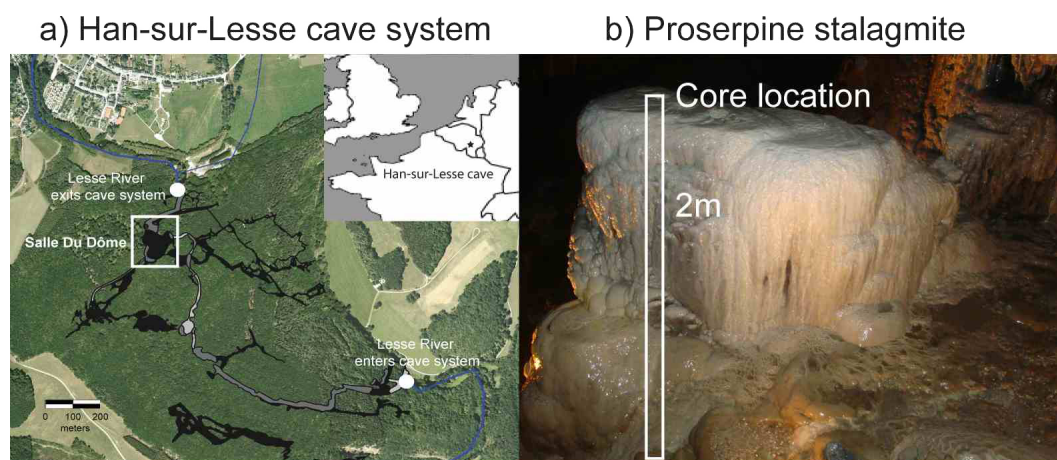
Figure 1. (a) The Han-sur-Lesse cave system is located in the southern part of Belgium. The Proserpine stalagmite was sampled in the Salle-du-Dôme chamber (white square), located 500 m from the cave exit. **(b)** The Proserpine stalagmite with the location of the 2 m long core that was drilled in 2001 at the spot where most of the drip water falls.

cipitation (PCP) intensity, driven by changes in effective precipitation. At a seasonal scale the $\delta^{18}O$ and $\delta^{13}C$ signals display an opposite behavior, with more negative $\delta^{18}O$ values in summer, when the $\delta^{13}C$ values are less negative (Van Rampelbergh et al., 2014).

3 Methods

The Proserpine stalagmite was sampled in January 2001 by drilling a 10 cm wide, 2 m deep core. The precise location for the drilling was on the side with the highest drip rate but far enough away from the edge to avoid disturbance of the expected horizontal layering of the growth increments (Fig. 1b). The core was cut in half and a slab of 1 cm was cut from the center. The slabs were polished by hand with carbide powder and finished with Al_2O_3. The upper 56 cm was further studied and cut into seven parts, numbered I to VII (Fig. 2), to allow easy handling in the laboratory. Layers were counted per part under a Merchantek MicroMill microscope and on high-resolution scans using Adobe Illustrator. To increase the reliability of the layer counting, layers were counted by different researchers, on different days and with different zooms when done on a computer screen. The reported layer amount is given by the average of 10 layer-counting rounds per part. The thickness of each layer was measured using the measurement tool of the Merchantek MicroMill microscope with an uncertainty of 0.1 μm. Samples for $\delta^{18}O$ and $\delta^{13}C$ measurements were taken with a drill bit of 0.3 mm diameter mounted on the Merchantek MicroMill. Ethanol was used to clean the speleothem surface and drill bit prior to sampling. Between samplings, the drill bit and speleothem surface were cleaned with compressed air. Samples were drilled every 0.5 mm in part I and in every layer for the other parts, in total 867 samples. Stable isotope measurements were carried out using a Kiel III device coupled

on a Thermo Delta plus XL with analytical uncertainties ≤ 0.12 ‰ for $\delta^{13}C$ and ≤ 0.16 ‰ for $\delta^{18}O$. A total of 20 U-series age, among which 8 from a previous study (Verheyden et al., 2006) were measured at the University of Minnesota (USA) using the procedures for uranium and thorium as described in Edwards et al. (1987) and Cheng et al. (2000, 2009a, b). StalAge (Scholz and Hoffmann, 2011) was used to interpolate the ages between the U / Th-age points. The seasonal character of the layering (Verheyden et al., 2006; Van Rampelbergh et al., 2014) in the Proserpine allows for layer counting to be used to establish an age model. The number of counted layer couplets per part represents the number of years for that part. The number of years obtained by layer counting is then compared with the number of years suggested by the U / Th ages per part. Results of both independent dating methods are combined to provide the final age model. The uncertainties (2σ) on all reported values correspond to a 95 % confidence interval and are calculated according to the following relation:

$$\bar{x} - t_{0.05,\,n-1} \cdot \frac{s}{\sqrt{n}} \leq \bar{x} \leq \bar{x} + t_{0.05,\,n-1} \cdot \frac{s}{\sqrt{n}},$$

where $\bar{x}$ is the arithmetic mean of the results, n the number of replicates, t the Student distribution function and s the standard deviation on the results. If $n \geq 30$, t approximates a normal distribution and is roughly equal to 2.

4 Results

Layering is present in the studied upper 56 cm of the Proserpine core and is formed by alternating dark (more compact) and white (more porous) layers. The seasonal character of the layering in the Proserpine stalagmite, with one dark and one white layer deposited every year, is suggested by Verheyden et al. (2006) and further confirmed by monitoring

Table 1. U / Th measurements (University of Minnesota) of the Proserpine stalagmite. All ages are converted to before 2013. Ages number 1, 2, 7, 8, 15, 17, 18 and 19, marked in bold, are the U / Th ages from Verheyden et al. (2006). The error is 2σ error.

Sample number	Stal. part	Distance (mm)	^{238}U (ppb)	^{232}Th (ppt)	^{230}Th/^{232}Th (atomic $\times 10^{-6}$)	δ^{234}U[a] (measured)	^{230}Th/^{238}U (activity)	^{230}Th age (yr) (uncorrected)	^{230}Th age (yr) (corrected)[b]	^{230}Th age (yr AD) (corrected)
1	**I**	**15**	**154.2 ± 0.1**		**5.2 ± 0.2**	**1390.7 ± 1.8**	**0.0036 ± 0.0002**	**164 ± 8**	**42 ± 70**	**1971 ± 70**
2	**I**	**60**	**118.6 ± 0.2**		**9.8 ± 0.4**	**1396 ± 4**	**0.0043 ± 0.0002**	**194 ± 7**	**119 ± 44**	**1894 ± 44**
3	I	86	66.8 ± 0.1	1444 ± 29	9 ± 1	1382.8 ± 3.3	0.0118 ± 0.0003	540 ± 13	276 ± 187	1737 ± 187
4	II	112	52.4 ± 0.1	260 ± 5	20 ± 1	1400.4 ± 4.2	0.0060 ± 0.0003	275 ± 13	215 ± 45	1798 ± 45
5	II	130	42.9 ± 0.1	124 ± 3	36 ± 2	1393.0 ± 5.6	0.0063 ± 0.0004	288 ± 17	253 ± 30	1760 ± 30
6	III	195	41.4 ± 0.1	316 ± 6	20 ± 1	1275.9 ± 3.7	0.0091 ± 0.0004	435 ± 17	337 ± 71	1676 ± 71
7	**IV**	**245**	**42.6 ± 0.1**		**44 ± 2**	**1329.4 ± 2.3**	**0.0087 ± 0.0004**	**408 ± 17**	**379 ± 30**	**1634 ± 30**
8	**IV**	**275**	**57.2 ± 0.1**		**41 ± 2**	**1347.7 ± 4.1**	**0.0092 ± 0.0004**	**430 ± 18**	**396 ± 30**	**1617 ± 30**
9	IV	332	65.3 ± 0.1	171 ± 4	55 ± 2	1309.7 ± 4.2	0.0087 ± 0.0003	411 ± 12	378 ± 26	1635 ± 26
10	V	342	55.1 ± 0.1	83 ± 2	94 ± 3	1395.5 ± 3.2	0.0086 ± 0.0002	393 ± 11	374 ± 17	1639 ± 17
11	V	360	38.8 ± 0.1	173 ± 4	38 ± 1	1401.4 ± 4.4	0.0103 ± 0.0003	469 ± 15	415 ± 41	1598 ± 41
12	V	399.2	44.6 ± 0.1	167 ± 3	48 ± 2	1398.5 ± 3.2	0.0108 ± 0.0003	494 ± 15	449 ± 35	1564 ± 35
13	VI	433.5	40.6 ± 0.1	72 ± 2	98 ± 4	1394.2 ± 4.3	0.0106 ± 0.0004	482 ± 18	460 ± 23	1553 ± 23
14	VI	493.5	43.7 ± 0.1	86 ± 2	91 ± 4	1406.2 ± 3.7	0.0109 ± 0.0004	495 ± 17	471 ± 24	1542 ± 24
15	**VI**	**510**	**46.7 ± 0.1**		**185 ± 19**	**1402.9 ± 4.2**	**0.0096 ± 0.0005**	**439 ± 23**	**440 ± 24**	**1573 ± 24**
16	VII	518	38.6 ± 0.1	79 ± 2	88 ± 4	1402.9 ± 4.5	0.0109 ± 0.0005	497 ± 23	472 ± 29	1541 ± 29
17	**VII**	**530**	**52.3 ± 0.1**		**184 ± 11**	**1409.8 ± 3.0**	**0.0101 ± 0.0004**	**459 ± 18**	**460 ± 19**	**1553 ± 19**
18	**VII**	**540**	**52.6 ± 0.1**		**188 ± 11**	**1392.8 ± 3.3**	**0.0105 ± 0.0004**	**481 ± 18**	**482 ± 19**	**1531 ± 19**
19	**VII**	**560**	**47.5 ± 0.1**		**219 ± 19**	**1394.9 ± 4.2**	**0.0113 ± 0.0005**	**515 ± 22**	**517 ± 23**	**1496 ± 23**
20	VII	560	45.9 ± 0.1	42 ± 1	208 ± 10	1384.7 ± 4.1	0.0115 ± 0.0004	525 ± 20	514 ± 21	1499 ± 21

U decay constants: $\lambda_{238} = 1.55125 \times 10^{-10}$ (Jaffey et al., 1971) and $\lambda_{234} = 2.82206 \times 10^{-6}$ (Cheng et al., 2000). Th decay constant: $\lambda_{230} = 9.1705 \times 10^{-6}$ (Cheng et al., 2013). [a] δ^{234}U = ([^{234}U / ^{238}U]$_{activity}$ − 1) × 1000. [b] δ^{234}U$_{initial}$ was calculated based on ^{230}Th age (T), i.e., δ^{234}U$_{initial}$ = δ^{234}U$_{measured}$ × e$^{\lambda234 \times T}$. Corrected ^{230}Th ages assume the initial ^{230}Th / ^{232}Th atomic ratio of $4.4 \pm 2.2 \times 10^{-6}$; those are the values for a material at secular equilibrium, with the bulk earth ^{232}Th / ^{238}U value of 3.8. The errors are arbitrarily assumed to be 50 %.

results of the Proserpine growth site (Van Rampelbergh et al., 2014). The Proserpine stalagmite displays a clear sedimentological perturbation between 9 and 10 cm (Fig. 2). During this perturbation, calcite deposition is heavily disturbed with straw pieces embedded in the calcite, which might be relics from fires lit on the paleo-surface of the stalagmite to illuminate the Salle-du-Dôme (Verheyden et al., 2006). Apart from this sedimentological perturbation, no features were found that could be interpreted as signs of interruptions ("hiatuses") of the continuous sedimentation. Even though layering is less clearly visible in certain parts, due to the calcite aspect, or where the sub-horizontal layering is strongly disturbed, there were always parts, apart from the perturbation between 9 and 10 cm, across the 10 cm width of the slab where the continuity of the layering was clearly visible throughout the full length of the core. Four proxies were measured on the Proserpine stalagmite: calcite aspect, layer thickness, and δ^{18}O and δ^{13}C values. Layer thickness varies between 0.05 and 1.7 mm layer^{-1} (Fig. 3) and dark layers are on average 0.05 mm thinner than white layers. The δ^{18}O values average -6.9 ± 0.16 ‰, and the δ^{13}C values average -10 ± 0.12 ‰. Four intervals characterized by large-amplitude variations in the four measured proxies occur between 7 and 8 cm, between 10.5 and 12.4 cm, between 18 and 20 cm, and between 34 and 36 cm (blue lines, Fig. 3). Between 7 and 8 cm and between 34 and 36 cm, calcite aspect is dark and compact with almost no visible layering. During these two intervals, layer thickness decreases to 0.2 mm layer^{-1} and the δ^{18}O and δ^{13}C values increase to values around -6.0 ± 0.16 and -8.0 ± 0.12 ‰, respec-

tively. Between 10.5 and 12.4 cm, calcite is heavily altered and is more matte and whiter compared to the generally more translucent calcite aspect of the Proserpine stalagmite. The heat of the fires made on the surface of the stalagmite during the perturbation period may have altered the calcite in this part. In this interval, layer thickness decreases to 0.2 mm layer^{-1} and the δ^{18}O and δ^{13}C values increase to values around -6.0 ± 0.16 and -6.5 ± 0.12 ‰, respectively. From 18 to 20 cm, layering is heavily undulating with vertically orientated layers in some parts, which may reflect small basin or rimstone structures. In this interval, layer thickness decreases to 0.4 mm layer^{-1} and the δ^{18}O and δ^{13}C values increase sharply to -6.2 ± 0.16 and -7.0 ± 0.12 ‰, respectively. With the exception of the four intervals characterized by simultaneous large-amplitude variations in the four measured proxies, the time series can be subdivided in two parts. For the part above the perturbation (part I), calcite aspect is generally darker and more compact. The δ^{18}O values average -6.6 ± 0.16 ‰ and δ^{13}C values average -10 ± 0.12 ‰. Both display a good correlation as indicated by a Spearman correlation coefficient of $\rho = 0.811$ ($p = 8.86 \times 10^{-44}$). Layer thickness in part I averages 0.3 mm layer^{-1} and displays similar variations to the isotopes with thicker layers corresponding to more negative isotopic values. The parts below the perturbation (parts II to VII) display more negative δ^{18}O values at -7.0 ± 0.12 ‰, while the δ^{13}C values vary around the same mean of -10 ± 0.12 ‰. A lower Spearman correlation coefficient between the δ^{18}O and δ^{13}C signals is calculated for these parts (parts II to VII; $\rho = 0.37$, $p = 9.54 \times 10^{-24}$). Below the perturbation, layer thickness
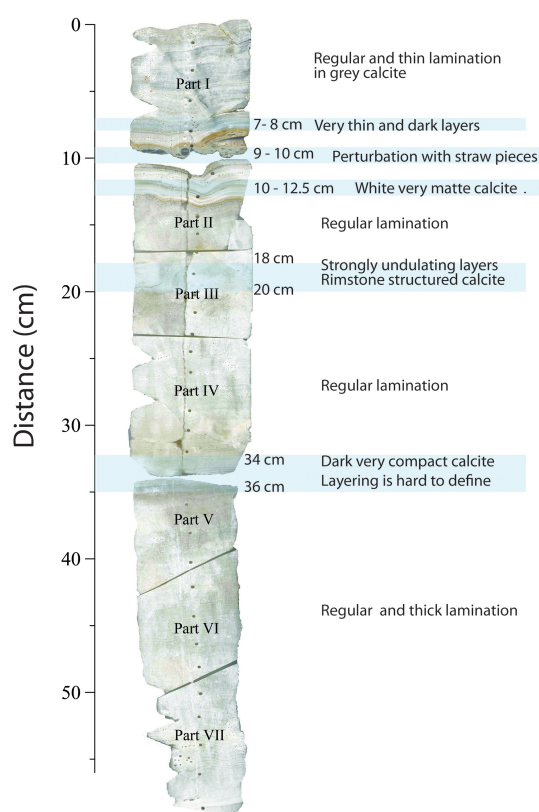
Figure 2. The upper laminated 56 cm of the Proserpine core with the description of the calcite aspect. The blue bars indicate intervals during which calcite deposition is disturbed or calcite aspect is very dark and compact or white and matte.

varies between 0.5 and 1 mm layer^{-1} and displays similar variations to the δ^{18}O values. In the lower section of part II and upper section of part III (14–18.5 cm) and for most of part V, part VI and VII (38–56 cm), the δ^{18}O signal is generally more negative (-7.5 ± 0.16 ‰) and the layer thickness increases to 0.8 mm layer^{-1} (Fig. 3). In the lower section of part III and in part IV (18.5 and 38 cm), the δ^{18}O values increase to -6.6 ± 0.16 ‰ and the layer thickness decreases to 0.5 mm layer^{-1}, while no general particular change is observed for the δ^{13}C values. Sampling for the stable isotopes was done layer per layer in parts II to VII and reflects seasonal variations in the δ^{18}O and δ^{13}C signals (for a high-resolution picture of the seasonally resolved isotope records, we refer the reader to Fig. 4 in Van Rampelbergh et al., 2014). The δ^{13}C seasonality evolves differently from the δ^{18}O seasonality. A larger δ^{18}O seasonality of 0.5 ‰ occurs in the lower section of part II and upper section of part III (14–18.5 cm) and for most of parts V, VI and VII (38–56 cm), while in the lower section of part III to IV (18.5–32 cm), the δ^{18}O seasonality lowers to 0.25 ‰. For δ^{13}C, the overall seasonality averages 0.7 ‰. An increase in δ^{13}C seasonality to 1.5 ‰ occurs at 32 cm and is followed by a gradual decrease until 27 cm, where the seasonality returns to 0.7 ‰.

Eight U / Th ages that were previously published in Verheyden et al. (2006) are used and numbered 1, 2, 7, 8, 15, 17, 18 and 19 and marked in light grey in Table 1. Twelve new U / Th ages measured in this study are listed in bold in Table 1 and correspond well to the previously measured ages. Layer-counting ages were carried out per part (i.e., parts I to VII) and are listed in Table 2 (column 5) together with their 2σ uncertainty range. To compare the two independent age methods (layer-counting method and U / Th-age method), the U / Th-age points have to be interpolated to obtain an age for the top and bottom of each part. The interpolation of the measured U / Th ages was carried out using StalAge and top and bottom ages of each part are listed in Table 2 (column 3). The difference between the top and bottom age of each part provides the number of years of that part (Table 2, column 4). The number of years per part derived from the U / Th ages display larger 2σ uncertainties for parts I, II and III (~ 70) compared to parts IV to VII, where uncertainties are smaller (~ 30). The number of years per part derived from the layer counting display 2σ uncertainties of ~ 7, which is smaller than the uncertainties in the U / Th ages. The obtained number of layers per part agrees for the two methods in parts I, II, II, V and VII. Note that the U / Th-age method suggests a much smaller number of years (Table 2, columns 4 and 5) in parts IV and VI.

The growth rates per part derived from the U / Th ages are listed in Table 2, column 6. The growth rates per part derived from the layer-counting ages are listed in Table 2, column 7. The growth rates per part based on layer counting increase in two steps: they are low at 0.6 mm yr^{-1} in part I; higher around 1 mm yr^{-1} in parts II, III and IV; and very high at 2 mm yr^{-1} in parts V, VI, and VII. The growth rates per part derived from the U / Th ages display much larger variations between the different parts, with exceptionally high growth rates of 5.6 mm yr^{-1} for part IV and 6.5 mm yr^{-1} for part VI.

5   Discussion

5.1   Speleothem age model

Two independent geochronological methods are used to establish the age model of the Proserpine: StalAge based on 20 U / Th ages and layer counting. Due to the interruption in calcite deposition between 9 and 10 cm, the layer-counting ages cannot be used to count the years back from the present until 56 cm. Apart from this interruption in deposition, the continuous layering was visible, at least in part, throughout the full length of the core across the 10 cm width of the slab. The absence of visible indications of interruptions in deposition, the high growth rate on the order of 1 mm per year, and the present-day high drip rate encouraged us to use layer counting as a reliable and precise geochronological approach. Moreover we could rely on previous work by Van Rampelbergh et al. (2014) that demonstrated that all layer duplets, consisting of a lighter and a darker one, correspond
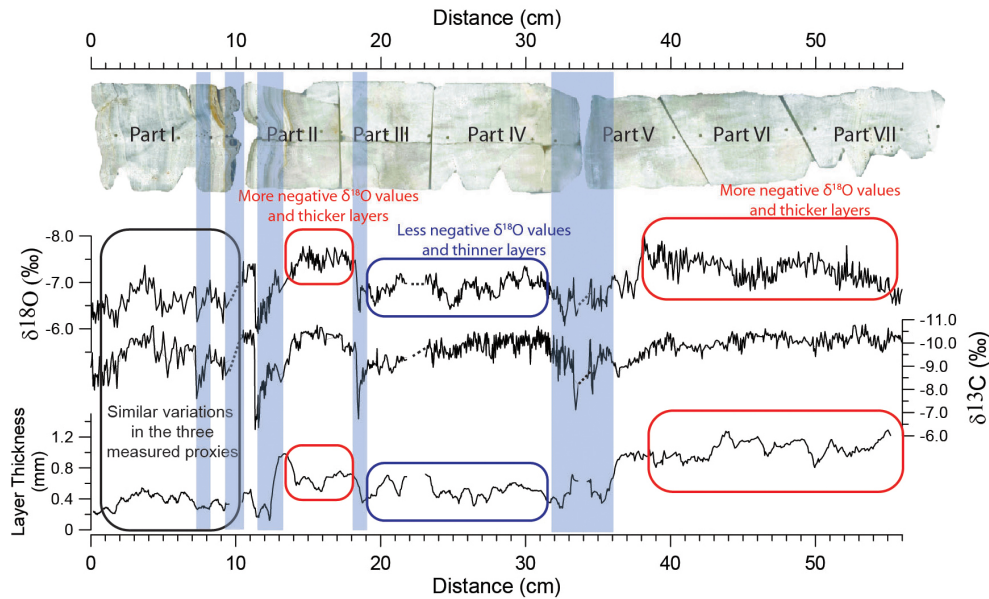
Figure 3. The δ^{18}O and δ^{13}C signals (‰ VPDB) and layer thickness of the Proserpine core plotted against distance from top. Blue bars indicate intervals during which the calcite aspect, δ^{18}O and δ^{13}C signals, and layer thickness all display simultaneous large-amplitude variations.

Table 2. Comparison between the layer-counting ages and U / Th ages per part together with their growth rates. The interpolated U / Th ages for the top and the bottom of each part were obtained using StalAge. All values are reported with their 2σ uncertainty range.

Part	Depth (cm)	U / Th ages interpolated years AD $\pm 2\sigma$	Amount of years U / Th ages per part years $\pm 2\sigma$	Amount of years layer counting per part years $\pm 2\sigma$	Growth rate U / Th ages (mm yr^{-1})	Growth rate layer counting (mm yr^{-1})
I	0	2001 $\pm$ 0				
	9	1822 $\pm$ 60	179 $\pm$ 60	144 $\pm$ 6	0.5 $\pm$ 0.2	0.6 $\pm$ 0.03
II	10	1810 $\pm$ 48				
	16.2	1723 $\pm$ 73	87 $\pm$ 87	66 $\pm$ 6	0.7 + 0.7	0.9 $\pm$ 0.08
III	16.2	1717 $\pm$ 70				
	22.4	1655 $\pm$ 33	62 $\pm$ 77	41 $\pm$ 5	1.0 + 1.2	1.5 $\pm$ 0.20
IV	22.4	1650 $\pm$ 29				
	33.6	1631 $\pm$ 16	19 $\pm$ 33	105 $\pm$ 7	5.9 $\pm$ 1	1.1 $\pm$ 0.01
V	33.6	1629 $\pm$ 15				
	41.3	1567 $\pm$ 21	62 $\pm$ 25	48 $\pm$ 4	1.3 $\pm$ 0.5	1.6 $\pm$ 0.13
VI	41.3	1567 $\pm$ 22				
	50	1553 $\pm$ 16	13 $\pm$ 27	42 $\pm$ 10	6.5 $\pm$ 13	2.1 $\pm$ 0.5
VII	50	1553 $\pm$ 16				
	56	1501 $\pm$ 17	53 $\pm$ 23	27 $\pm$ 8	1.1 $\pm$ 0.5	2.2 $\pm$ 0.6

to 1 year. To compare the U / Th ages and the layer-counting ages, the number of years must be determined for each part (Table 2, columns 4 and 5). Results show that the layer-counting method displays smaller uncertainties. Both independent geochronological methods deliver similar ages, with the exception of parts IV and VI, where the U / Th ages suggest a lower number of years. The U / Th ages indicate that part IV was deposited in 19 ± 33 years, while the layer counting indicates a total of 105 ± 7 years (Table 2). The U / Th ages suggest that part VI was deposited in 13 ± 27 years, while the layer counting indicates a total of 42 ± 10 years

(Table 2). The number of years obtained by layer counting in the two parts IV and VI is considered more probable compared to the number of years obtained by U / Th ages. Based on in situ monitoring of the Proserpine drip site demonstrating the seasonal character of the layering and the good agreement of the layer counting and the U / Th ages in most of the other parts, the layer-counting model is seen as the most accurate to establish the chronology. Furthermore, the U / Th ages give improbably high growth rates (~ 6 mm yr^{-1}) for parts IV and VI (Table 2).
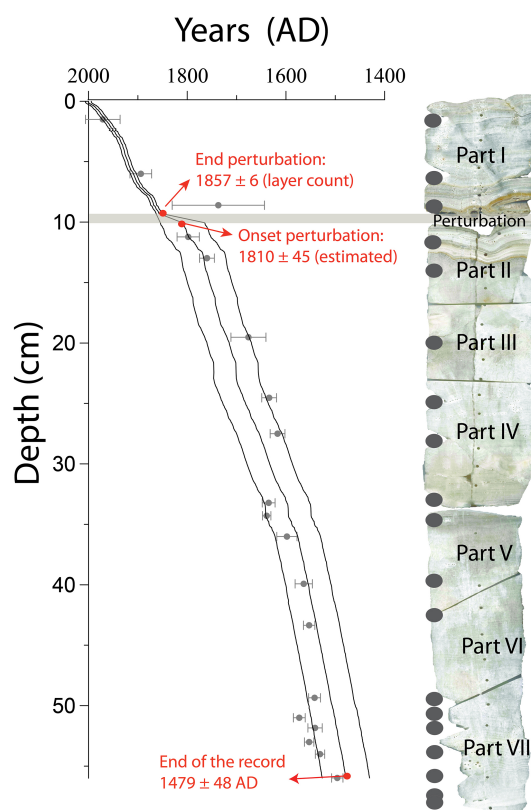
Figure 4. Age–depth model of the Proserpine based on layer-counting ages reported with their 2σ uncertainty. The onset of the perturbation is estimated by counting the layers back up from the U / Th age located closest below the perturbation. U / Th ages are plotted in light grey in the age–depth graph with their 2σ uncertainty. Location of U / Th samples on the Proserpine core is indicated by the black dots. All ages are reported in years AD.

The Proserpine age model is subdivided into two parts by means of the layer-counting ages: the part above the perturbation and the part below the perturbation. The age of part I above the perturbation can be obtained by simply counting the layers back from 2011. This leads to an age of AD 1857 ± 6 for the end of the perturbation (Fig. 4). Below the perturbation (at 10 cm), the age of the onset of the perturbation has to be estimated in order to restart the layer counting downwards. This is carried out by counting the layers back upward from the U / Th age located closest below the perturbation (i.e., AD 1798 ± 45). By doing this, a total of 12 ± 2 layer-couplets are obtained, indicating that the age of the onset of the perturbation is estimated to be AD 1810 ± 45 (Fig. 4). The good estimation of this age is confirmed by the fact that StalAge suggests an age of AD 1810 ± 48 for the onset of the perturbation. Furthermore, a ^{14}C date on a straw piece embedded in the perturbed calcite indicates an age interval of 1760 to 1810 (probability of 95.4 %; Verheyden et al., 2006), also suggesting a similar time window for the perturbation. The age of AD 1810 ± 45 is consequently

Table 3. Uncertainties in the counted layers per part below the perturbation (II to VII) together with the uncertainties in the obtained ages (AD) per part using the age of AD 1810 ± 45 as the starting point for the age model counting.

Part	Uncertainty in counted layers per part $\pm 2\sigma$	Uncertainty in obtained ages (AD) per part $\pm 2\sigma$
II		Starting point (AD 1810 ± 45)
	± 6	± 45
III	± 5	± 45
IV	± 7	± 46
V	± 4	± 46
VI	± 10	± 47
VII	± 8	± 48

considered a good estimation of the onset of the perturbation. This age is used to restart layer counting downwards. Since the uncertainties in the layer-counting ages are determined per part, the uncertainty in the age model increases per additional older part according to the propagation of uncertainties in a sum (Table 3). The age obtained for the bottom of the laminated part of the Proserpine stalagmite at 56 cm is AD 1479 ± 48 (Fig. 4).

5.2 Factors driving decadal and multidecadal changes in the measured proxies

Variations in δ^{18}O values of speleothems deposited in equilibrium with their drip water relate mainly to changes in air temperature, rainfall amount and/or source of the rainfall (Fairchild et al., 2006). Rainfall sources often imply δ^{18}O shifts on the order of several per mill (Fleitmann et al., 2007), while the δ^{13}C values and layer thickness values remain unchanged. The large-scale δ^{18}O variations in the Proserpine are on the order of 1 to 2 ‰ and always occur together with large-scale δ^{13}C variations on the same order and a decrease in layer thickness, indicating that the source effect is most probably not responsible for these δ^{18}O variations. In temperate regions, speleothem δ^{18}O values often display complicated relations with surface air temperature due to the inverse effect of temperature on the rainwater δ^{18}O compared to the calcite δ^{18}O. The relation between surface air temperature and rainwater δ^{18}O varies between ~ 0.1 and 0.3 ‰ per 1 °C for central Europe (Schmidt et al., 2007). The temperature-dependent fractionation during calcite formation within the cave acts in the opposite direction, and is around -0.2 ‰ per 1 °C for the Proserpine drip site as suggested by monitoring results (Van Rampelbergh et al., 2014). The net effect of air temperature changes on the Proserpine δ^{18}O signal may thus vary between ~ -0.1 and 0.1 ‰ per 1 °C considering that the temperature dependence of the rainwater of ~ 0.1 and 0.3 ‰ per 1 °C is also valid for Belgium. Consequently, the temperature effect most probably only has a minor influence on the decadal and multidecadal variations in the Proserpine δ^{18}O

signal. In the studied region, more positive δ^{18}O values have been observed to correspond to drier periods and thus reflect the amount effect (Verheyden, 2001). Variations in the Proserpine δ^{18}O may thus possibly relate to changes in wetter or drier conditions.

If recharge is seasonally biased, the decadal and multi-decadal δ^{18}O variations may be caused by variations in air temperature and/or by rainfall amount during a certain season. Hydrological studies of the Han-sur-Lesse epikarst show that recharge mostly occurs between spring and fall, with the largest amounts of recharge in winter (Bonniver, 2011). Rainfall δ^{18}O data show that winter rainfall has a more negative δ^{18}O value compared to the rainfall from other seasons (Van Rampelbergh et al., 2014). During periods of lower winter recharge, relatively more spring and fall waters with higher δ^{18}O are added to the epikarst reservoir. Therefore less negative δ^{18}O values are recorded in the speleothem. Periods of increased δ^{18}O values in the Proserpine record may thus be reflecting drier winter periods and vice versa. The relation between lower drip water δ^{18}O and higher winter recharge amounts can be illustrated by drip water monitoring data over several years. Although no such data are available, winter recharge is considered the main factor determining the δ^{18}O values of the Proserpine. More positive δ^{18}O values are interpreted to reflect drier winter periods and vice versa. Furthermore, a good Spearman correlation can be established between lower winter precipitation intensities (DJF) and lower winter temperatures (DJF) measured by the RMI since 1833 ($\rho = 0.47$ and $p = 3.99 \times 10^{-11}$), suggesting that drier winters correspond to colder winters. More negative δ^{18}O values in the Proserpine may thus possibly reflect drier winter conditions that are most probably also colder. A similar interpretation is used for the decadal and centennial δ^{18}O variations measured in a German speleothem with similar yearly temperature and yearly precipitation amounts to the Proserpine growth site (Wackerbarth et al., 2010; Fohlmeister et al., 2012).

Since no major vegetation changes (mainly C3 vegetation) occurred above the cave for the studied period and site, changes in δ^{13}C values might relate to changes in soil activity (Genty et al., 2003; Fohlmeister et al., 2012) and/or prior calcite precipitation (PCP; Fairchild et al., 2000). Plant CO_2 has a more negative δ^{13}C value than atmospheric CO_2 (δ^{13}C of C3 vegetation is between -20 and -25‰, while in atmospheric CO_2 it evolved from roughly -7 to -8‰ during the studied period). A reduced plant-CO_2 input in the soil due to lower soil activity will increase the δ^{13}C of the soil-CO_2 reservoir and consequently the δ^{13}C of the dissolved inorganic carbon (DIC) in the epikarst water. During PCP, calcite is deposited from the percolating epikarst water before entering the cave as drip water. This process mostly occurs during drier periods, when aerated zones become more important in the epikarst. PCP causes a simultaneous increase in the δ^{13}C and in the Mg / Ca and Sr / Ca composition of the drip water and speleothem calcite (Fairchild et al., 2000). Although

no Mg / Ca and Sr / Ca ratios are measured in the Proserpine, which makes it difficult to evaluate the process of PCP, monitoring results have clearly demonstrated that PCP is an important process in the Han-sur-Lesse epikarst (Van Rampelbergh et al., 2014). Both effects (soil activity and PCP) act in the same direction, and both cause the δ^{13}C values to increase during drier periods. Since drier periods in the cave are caused by lower winter recharge periods, increased δ^{13}C values are interpreted to reflect drier and most probably also colder winter periods. This interpretation is also supported by the observations made by Verheyden et al. (2014), and referred to in the Introduction, in a speleothem in the Père Noël cave, which is part of the same Han-sur-Lesse cave system, in which the similarly varying isotopic (δ^{18}O and δ^{13}C) and geochemical (Mg / Ca and Sr / Ca) proxies could be interpreted in terms of alternations of wetter and drier phases, causing changes between weaker or absent PCP and more intense PCP, respectively.

Disequilibrium processes due to a stronger pCO$_2$ gradient between the cave air and drip water and/or due to longer drip intervals may cause simultaneously increased δ^{18}O and δ^{13}C values (Mühlinghaus et al., 2009; Scholz et al., 2009; Deininger et al., 2012). Under present-day conditions, pCO$_2$ levels of the cave air in the Salle-du-Dôme are low year-round and equal the outside air values. pCO$_2$ levels may change over time due to changes in ventilation patterns, which may change over time due to new cave openings. No such new openings that may have affected the Salle-du-Dôme ventilation have occurred in the last 500 years. The effect of the changing pCO$_2$ gradient on the drip water δ^{18}O and δ^{13}C values over the studied period is thus unlikely. Longer drip intervals due to decreased drip flow may be possible. However, under present-day conditions, a continuous high drip water flow feeds the stalagmite, which inhibits disequilibrium effects related to longer drip interval (Mühlinghaus et al., 2009). The drip discharge consequently needs to have sufficiently decreased, beneath a certain threshold value, to allow for disequilibrium processes to occur. Since recharge occurs in winter (Bonniver, 2011), a decreased drip discharge is expected to relate to significantly drier winters that are most probably also colder. Furthermore, during periods of lower drip discharge, PCP will occur and further increase the δ^{13}C signal. Decreased drip discharge due to significantly drier (and colder) winters will consequently cause increased correlation in δ^{18}O and δ^{13}C values, with a larger increase in δ^{13}C values compared to the δ^{18}O values, the latter being not affected by PCP.

Layer thickness and calcite aspect in the Proserpine are expected to relate to growth rate, with thinner layers and darker calcite formed under slower growth. Growth rate is primarily dependent on two factors: the discharge amount, which is expected to lower during drier (and colder) winter periods, and the cave seepage water calcium ion concentration (Genty et al., 2001). The cave seepage water calcium ion concentration depends on mainly two factors. The first fac-

tor, the soil pCO$_2$, is expected to increases during warmer and wetter periods. Higher soil pCO$_2$ increases the amount of CO$_2$ dissolved in the soil water. Water containing higher CO$_2$ amounts more easily dissolves CaCO$_3$, which increases its calcium ion concentration. The second factor determining seepage water calcium ion concentration is the intensity of PCP. PCP mostly occurs during dry periods and decreases the Ca^{2+} concentration of the drip water due to precipitation of calcite in the epikarst. Cave-monitoring results show that PCP is an important process in the Han-sur-Lesse epikarst that becomes more intense during the drier summer season (Van Rampelbergh et al., 2014). During drier periods, most probably caused by drier (and colder) winter periods, soil activity will decrease and PCP will increase, both causing lower calcium ion concentration of the drip water. A lower calcium ion concentration and a lower drip discharge during drier (and colder) winters will both cause slower calcite deposition and consequently thinner layers and darker calcite.

To conclude, decadal and centennial changes in the proxies (δ^{18}O and δ^{13}C signals, layer thickness and calcite color) reflect changes in drier (and colder) versus wetter (and warmer) winters. Exceptionally dry (and cold) winters shift the drip discharge below a certain threshold value, which causes the proxies to display simultaneous large-amplitude shifts. During such exceptionally dry (and cold) winter periods, the δ^{18}O and δ^{13}C values increase, layer thickness decreases and calcite aspect becomes darker and/or disturbed. When the discharge threshold is not reached, calcite is deposited close to equilibrium and the four proxies may vary independently.

5.3 Anomalies in the proxy records

Proserpine calcite deposited in equilibrium with its drip water has a δ^{18}O value of -6.7 ± 0.16 ‰ and a δ^{13}C value of -10 ± 0.12 ‰ (Van Rampelbergh et al., 2014). Four periods where the δ^{18}O and δ^{13}C values abruptly increase away from the present-day equilibrium occur in the Proserpine from 1565 to 1610, at 1730, from 1770 to 1800, and from 1880 to 1895 and are interpreted as anomalies in the record (blue bars, Fig. 5). During these anomalies layer thickness decreases below 0.2 mm layer^{-1} and calcite aspect is disturbed or very dark and compact. As indicated by the detailed analysis of the climatic factors affecting the different used proxies, as soon as a certain threshold value is reached, the four proxies display simultaneous large-amplitude changes and reflect exceptionally dry (and cold) winter periods. No calcite was deposited between 1810 and 1860, which strongly suggests that too little water was dripping on the Proserpine during that period. Therefore, this period is also interpreted as an anomaly reflecting exceptionally dry (and cold) winters. A total of five anomalies are suggested by the Proserpine proxies and last between 1565 and 1610, at 1730, between 1770 and 1800, between 1810 and 1860, and between 1880 and 1895 (blue bars, Fig. 5). The five anomalies suggesting exceptionally dry (and cold) winter conditions correspond to

known cold and/or dry periods in historical and instrumental archives and in winter temperature reconstructions from Europe and central Europe (Fig. 5):

– Between 1565 and 1610, winter temperatures in Europe (Luterbacher et al., 2004) and central Europe (Dobrovolny et al., 2010) were low (Fig. 5f and g). Historical data of France, Belgium and the Netherlands indicate icy cold winters; harsh famines; low numbers of child births and weddings; and the outbreak of the plague, with its worst years from 1562 to 1570 (Le Roy Ladurie, 2004). The shift to cold and dry conditions at AD 1565 is interpreted as the onset of the second pulse of the Little Ice Age (LIA, $\pm$1300–1850; Le Roy Ladurie, 2004) and is nicely recorded in the Proserpine proxies as a shift to drier (and colder) winters. Between 1590 and 1600, the Proserpine proxies suggest a shorter wetter (and warmer) interval as indicated by the more negative δ^{18}O and δ^{13}C values and thicker layers (Fig. 5a, b and c). A similar decade of warmer conditions between 1590 and 1600 is also reported in winter temperature reconstructions from Europe (Luterbacher et al., 2004) and central Europe (Dobrovolny et al., 2010) and from historical archives (Le Roy Ladurie, 2004).

– At 1730, the abrupt shift in the measured proxies suggests a short but exceptionally dry (and cold) winter period. Considering the age uncertainty of $\pm$45 years for this period (Fig. 5), the dry (and cold) conditions suggested by the Proserpine at AD 1730 $\pm$ 45 most probably relate to the exceptionally cold and dry decade between AD 1690 and 1700 recorded in historical archives (Le Roy Ladurie, 2004) and by extremely low winter temperatures in Europe (Luterbacher et al., 2004) and central Europe (Dobrovolny et al., 2010; Fig. 5f and g).

– Between 1770 and 1800, the Proserpine proxies suggest a dry (and cold) winter period that corresponds to a known period of colder winters in Europe (Fig. 5f and g; Le Roy Ladurie, 2004; Luterbacher et al., 2004; Dobrovolny et al., 2010).

– The exceptionally dry (and cold) winter conditions between 1810 and 1860, as suggested by the Proserpine, correspond nicely to decreased winter temperatures in Europe (Luterbacher et al., 2004) and central Europe (Dobrovolny et al., 2010; Fig. 5f and g). Historical climate data from France, Belgium and the Netherlands indicate that this interval corresponds to the third and last cold pulse of the LIA and is characterized by exceptionally cold winters and warm summers (Le Roy Ladurie, 2004).

– The most recent dry (and cold) period recorded in the Proserpine (1880 and 1895) corresponds to colder winter temperatures and lower winter precipitation amounts
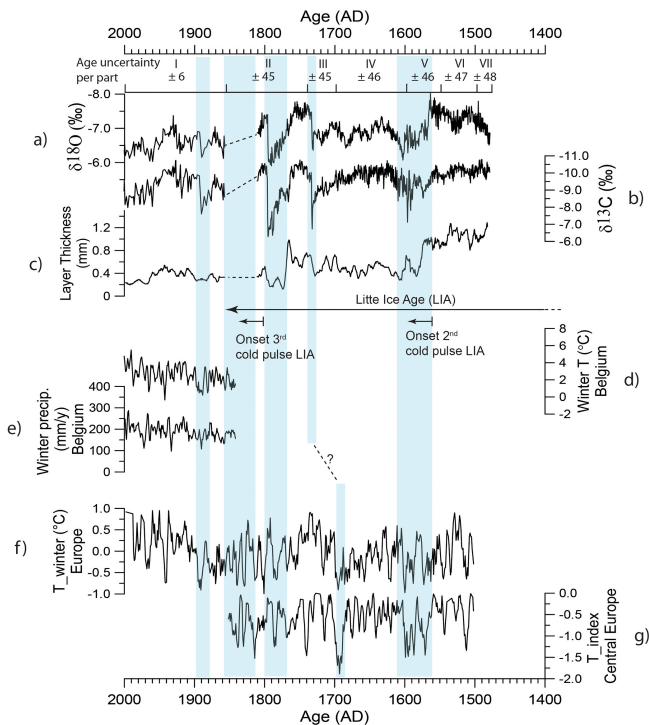
Figure 5. (a) δ^{18}O and **(b)** δ^{13}C values (‰ VPDB) and **(c)** layer thickness plotted against **(d)** the instrumental winter temperature (DJF) and **(e)** winter precipitation (DJF) record of the Belgian Royal Meteorological Institute (RMI) measured in Brussels since 1833, **(f)** the winter temperature reconstruction based on multiple proxies in Europe (Luterbacher et al., 2004) and **(g)** the winter temperature reconstruction derived from documentary and instrumental evidence in central Europe (Dobrovolny et al., 2010). Five exceptionally dry (and cold) winter periods suggested by the Proserpine are indicated by blue bars and correspond to clear cold periods in instrumental records and winter temperature reconstructions in Europe and central Europe. Two periods of relatively wetter (and warmer) winters occur from 1479 and 1565 and from 1730 to 1770 and correspond to known warmer intervals. Between 1610 and 1730 the Proserpine suggests relatively drier (and colder) winter periods, which correspond to colder winter conditions in Europe and central Europe.

as measured by the RMI in Belgium since 1833 (Fig. 5d and e). The temperature drop is clearly visible in the winter temperature reconstruction from Europe (Luterbacher et al., 2004; Fig. 5f). A decrease in precipitation has also been recorded in the England and Wales precipitation record, where this period is known as very dry with peak dry years at 1884, 1887 and 1893 (Nicholas and Glasspoole, 1931).

The exact forcing behind these five dry (and cold) winter periods is still a matter of discussion. The most trivial forcing of the western European climate is the variation in winter North Atlantic Oscillation (NAO; Trouet et al., 2009). During a negative winter NAO phase, westerlies winds are forced

over southern Europe, which may cause drier and colder winter conditions over Belgium. However, the five dry (and cold) winter periods observed in the Proserpine do not always correspond to negative winter NAO phases (Trouet et al., 2009). Other than negative NAO phases, lower solar irradiance combined with the input of volcanic ejecta in the atmosphere may also be responsible for decreased temperatures in Europe. Such is probably the case for the cold and dry period between 1810 and 1860 (third pulse of the LIA). In this period, solar insolation decreased during the Dalton Minimum (1790–1810; Mann, 2002) and the eruption of the Tamborra volcano (Indonesia) in 1815. A combination of negative NAO conditions (Luterbacher et al., 2001), the eruption of the Krakatoa volcano (Indonesia) in 1883 and lower sunspot activity (Lassen and Friischristensen, 1995) is most probably responsible for the exceptionally dry (and cold) winter period between 1880 and 1895.

5.4 More gentle alternations of warmer and wetter with colder and drier periods

In contrast to the five periods where large-amplitude anomalies of the four proxies suggest exceptionally dry (and cold) winter conditions, the remaining parts of the Proserpine stalagmite display more limited variations. Between 2001 and 1860, above the perturbation, the δ^{18}O and δ^{13}C values display a bulge with most negative values around 1930. Layer thickness follows the same evolution, with the thickest layers around 1930 indicating an evolution to wetter (and warmer) winters up to 1930 followed by an evolution to drier (and colder) winters up until 2001. This observation in the Proserpine proxies does not correspond to instrumental winter precipitation and temperature data measured by the RMI since 1833, nor does it with European winter temperature reconstructions (Luterbacher et al., 2004; Fig. 5). Calcite is darker in this part due to the incorporation of soot from torches used to illuminate the chamber during cave visits (Verheyden et al., 2006). Soot incorporation in the calcite structure may hamper the calcite deposition and overprint lower-amplitude climate variations. However, large-amplitude variations such as the dry (and cold) winter anomaly between 1880 and 1895 are still visible within this part, indicating that the climate signal is not fully overprinted. The possible effects of soot on δ^{18}O and δ^{13}C values and layer thickness need further investigation to allow for low-amplitude climate variations to be derived in the part above the perturbation.

Below the perturbation, and with exception of the anomaly periods, the measured proxy signals can be subdivided into three periods: between 1479 and 1565, between 1610 and 1730, and between 1730 and 1770 (Fig. 5a, b and c). Between 1479 and 1565 and between 1730 and 1770, more negative δ^{18}O values and thicker layers indicate relatively wetter (and warmer) winter conditions. In between the two latter periods (1610–1730), the δ^{18}O values become less negative and layers become thinner, indicating relatively drier (and cooler)
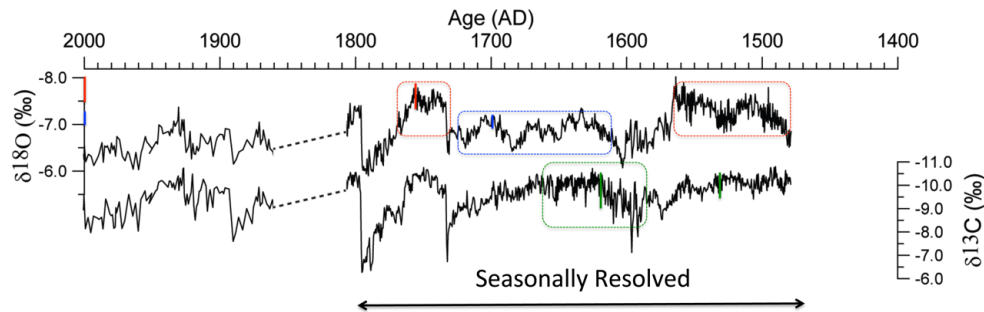
Figure 6. A decrease in δ^{18}O seasonality in the drier (and cooler) period between 1610 and 1730 (in blue) indicates lower cave air temperature seasonality than during the wetter (and warmer) periods (1479–1565 and 1730–1770) (in red). Seasonality in the δ^{13}C signal is higher between 1600 and 1660 and indicates more intense PCP during summer (in green), which is caused by decreased winter recharge. All values are in ‰ VPDB.

winter conditions. During the three abovementioned periods (1479–1565, 1610–1730, 1730–1770), the δ^{13}C values display no variations, indicating no major changes in soil activity or PCP intensity. Only during the relatively drier (and colder) winter period between 1610 and 1730 do the δ^{13}C values display a weak gradual increase (i.e., from 1700 to 1730). The relatively dry (and cool) conditions in the period between 1610 and 1730 may have caused lower soil activity and a gradual increase in prior calcite precipitation, which gradually augment the δ^{13}C signal.

The two periods with relatively wetter (and warmer) winters (1479–1565 and 1730–1770) interrupted by a period with drier (and cooler) winters (1610–1730) observed in the Proserpine are also recorded in the winter temperature reconstructions of Europe (Luterbacher et al., 2004) and central Europe (Dobrovolny et al., 2010; Fig. 5) and in historical archives (Le Roy Ladurie, 2004). The relatively drier (and cooler) winter period between 1610 and 1730 corresponds to colder winter conditions in Europe and central Europe and is referred to as the second pulse of the LIA (Le Roy Ladurie, 2004). This relatively cooler interval may relate to the Maunder Minimum, which was a period of decreased solar activity between 1640 and 1714. However, lower solar irradiance alone cannot be responsible for the cooler conditions between 1610 and 1730. The exact forcing of this second pulse of the LIA is still a matter of discussion.

5.5 Seasonality in δ^{18}O and δ^{13}C values

The δ^{18}O and δ^{13}C values were measured on a seasonal scale between 1479 and 1810 and clearly display seasonal variations (Fig. 6). The interpretation of the δ^{18}O and δ^{13}C variations on a seasonal scale strongly differs from the interpretation of these proxies on a decadal and multidecadal scale. Whereas the decadal and multidecadal variations in δ^{18}O and δ^{13}C vary in phase and reflect changes in drier (and colder) versus wetter (and warmer) winters, the seasonal δ^{18}O and δ^{13}C values vary in anti-phase. Seasonal δ^{18}O variations are driven by seasonal cave air temperature changes with a tem-

perature dependence of -0.2 ‰ per $1\,^\circ$C (Van Rampelbergh et al., 2014). Higher cave air temperatures in summer lead to lower δ^{18}O values of the formed calcite. The seasonal variation in δ^{13}C values is driven by the seasonal change in PCP intensity, with stronger PCP, due to drier conditions in summer leading to increased calcite δ^{13}C values (Van Rampelbergh et al., 2014).

The seasonality in δ^{18}O measured during the two wetter (and warmer) winter periods (1479–1565 and 1730–1770), equals 0.5 ‰, which is similar to the present-day conditions (Van Rampelbergh et al., 2014) and corresponds to a 2 to 2.5 $^\circ$C seasonality in cave air temperature. Between 1610 and 1730, winters are relatively drier (and cooler), and the δ^{18}O seasonality lowers to 0.25 ‰, corresponding to a 1 to 1.5 $^\circ$C cave air temperature seasonality. Lower summer temperatures during this cold LIA period are most probably responsible for the lower cave air seasonality.

The δ^{13}C signal mostly displays a seasonality of 0.7 ‰, which is smaller than the 1 ‰ seasonality in δ^{13}C values observed under the present-day conditions (Van Rampelbergh et al., 2014). At 1600, the δ^{13}C seasonality increases to 1.5 ‰ and displays a gradual decreasing trend back to 0.7 ‰ at 1660. The increase in δ^{13}C seasonality between 1600 and 1660 also corresponds to an interval where layers are thinner ($\sim 0.4\,\mathrm{mm\,layer^{-1}}$) but clearly alternating between dark and compact and white and porous layers. This suggests well-expressed wet winter conditions and dry summer conditions in the cave. The relatively drier (and colder) winter conditions in the period between 1610 and 1730 cause the yearly water recharge (occurring mostly in winter) to be lower compared to the two periods with wetter (and warmer) winters (1479–1565 and 1730–1770). A lower recharge during winter will consequently lead to drier cave conditions in summer and increase the effect of PCP. Increased PCP in summer due to lower winter recharge is interpreted to be responsible for the increased δ^{13}C seasonality and the clear layering between 1600 and 1660.

6   Conclusions

1. A multiproxy approach using δ^{18}O and δ^{13}C values, layer thickness and calcite aspect, in terms of dark and more compact vs. white and more porous, of the Proserpine stalagmite from the Han-sur-Lesse cave, Belgium, successfully reconstructs the climate over the last 522 years in terms of drier (and colder) versus wetter (and warmer) winters.

2. Thinner layers and darker calcite correspond to periods with decreased growth rate, driven by lower recharge and stronger PCP effects during drier (and colder) winters. More positive δ^{18}O values are interpreted to reflect drier (and colder) winters, due to the decreased input of winter recharge water with more negative isotopic composition. More positive δ^{13}C values reflect lower soil activity and increased PCP during drier (and colder) winter periods.

3. Anomalies in the measured proxies occur when discharge drops under a certain threshold value. During these anomalies, the δ^{18}O and δ^{13}C values increase away from isotopic equilibrium, layers become thin and the calcite becomes very dark or disturbed. Such periods occur between 1565 and 1610, around 1730, between 1770 and 1800, between 1810 and 1860, and between 1880 and 1895 and are interpreted as reflecting exceptionally dry (and cold) winter conditions. The exceptionally dry (and cold) periods found in the Proserpine speleothem correspond well to known dry and cold periods in historical, instrumental and/or temperature reconstruction records from Europe.

4. Less exceptional variations occur between 1479 and 1565 and between 1730 and 1770, with more negative δ^{18}O values and thicker layers reflecting two relatively wetter (and warmer) winters. Less negative δ^{18}O values, still reflecting equilibrium conditions, and thinner layers between 1610 and 1730 are interpreted to reflect a period of relatively drier (and cooler) winters. The two relatively wetter (and warmer) winter periods correspond to warmer periods in European winter temperature reconstructions and historical data from Belgium, the Netherlands and France. The drier (and cooler) winter period between 1610 and 1730 corresponds to relatively colder conditions in winter temperature reconstructions and historical data.

5. Seasonally resolved isotopic signals successfully record seasonal changes in cave air temperature and PCP. The δ^{18}O signals suggest a 2 to 2.5 °C cave air temperature seasonality between 1479 and 1565 and between 1730 and 1770, which is similar to the seasonality in cave air temperature observed today. Between 1610 and 1730, corresponding to a period with drier (and cooler) winters, the seasonality in cave air temperature decreases to

1 to 1.5 °C. The δ^{13}C seasonal changes suggest that the seasonality in discharge was lower than observed today, with a short interval of increased seasonality between 1600 and 1660 reflecting stronger summer PCP effects due to decreased winter recharge.

References

Baker, A., Wilson, R., Fairchild, I. J., Franke, J., Spoetl, C., Mattey, D., Trouet, V., and Fuller, L.: High resolution δ^{18}O and δ^{13}C records from an annually laminated Scottish stalagmite and relationship with last millennium climate, Global Planet. Change, 79, 303–311, 2011.

Boch, R., Spoetl, C., and Kramers, J.: High-resolution isotope record of early Holocene rapid climate change from two coeval stalagmites of Katerloch cave, Austria, Quaternary Sci. Rev., 28, 2527–2538, 2009.

Bonniver, I.: Etude Hyrogeologique et dimmensionnement par modelisation du "systeme-tracage" du reseau karstique the Han-sur-Lesse (Massif de Boine, Belgique), Geologie, FUNDP Namur, Namur, 93–97, 2011.

Cheng, H., Edwards, R. L., Hoff, J., Gallup, C. D., Richards, D. A., and Asmerom, Y.: The half-lives of uranium-234 and thorium-230, Chem. Geol., 169, 17–33, 2000.

Cheng, H., Edwards, R. L., Broecker, W. S., Denton, G. H., Kong, X., Wang, Y., Zhang, R., and Wang, X.: Ice Age Terminations, Science, 326, 248–252, 2009a.

Cheng, H., Fleitmann, D., Edwards, R. L., Wang, X. F., Cruz, F. W., Auler, A. S., Mangini, A., Wang, Y. J., Kong, X. G., Burns, S. J., and Matter, A.: Timing and structure of the 8.2 kyr BP event inferred from delta O-18 records of stalagmites from China, Oman, and Brazil, Geology, 37, 1007–1010, 2009b.

Deininger, M., Fohlmeister, J., Scholz, D., and Mangini, A.: Isotope disequilibrium effects: The influence of evaporation and ventilation effects on the carbon and oxygen isotope composition of speleothems – A model approach, Geochim. Cosmochim. Ac., 96, 57–79, 2012.

Dobrovolny, P., Moberg, A., Brazdil, R., Pfister, C., Glaser, R., Wilson, R., van Engelen, A., Limanowka, D., Kiss, A., Halickova, M., Mackova, J., Riemann, D., Luterbacher, J., and Boehm, R.: Monthly, seasonal and annual temperature reconstructions for Central Europe derived from documentary evidence and instrumental records since AD 1500, Climatic Change, 101, 69–107, 2010.

Edwards, R. L., Chen, J. H., and Wasserburg, G. J.: 238U-234U-230Th-232Th systematics and the precise measurement of time over the past 500 000 years, Earth Planet. Sc. Lett., 81, 175–192, 1987.

Fairchild, I. J., Borsato, A., Tooth, A. F., Frisia, S., Hawkesworth, C. J., Huang, Y. M., McDermott, F., and Spiro, B.: Controls on trace element (Sr-Mg) compositions of carbonate cave waters: implications for speleothem climatic records, Chem. Geol., 166, 255–269, 2000.

Fairchild, I. J., Smith, C. L., Baker, A., Fuller, L., Spötl, C., Mattey, D., McDermott, F., and E. I. M. F.: Modification and preservation of environmental signals in speleothems, Earth-Sci. Rev., 75, 105–153, 2006.

Fleitmann, D., Burns, S. J., Mangini, A., Mudelsee, M., Kramers, J., Villa, I., Neff, U., Al-Subbary, A. A., Buettner, A., Hippler, D., and Matter, A.: Holocene ITCZ and Indian monsoon dynamics recorded in stalagmites from Oman and Yemen (Socotra), Quaternary Sci. Rev., 26, 170–188, 2007.

Fohlmeister, J., Schröder-Ritzrau, A., Scholz, D., Spötl, C., Riechelmann, D. F. C., Mudelsee, M., Wackerbarth, A., Gerdes, A., Riechelmann, S., Immenhauser, A., Richter, D. K., and Mangini, A.: Bunker Cave stalagmites: an archive for central European Holocene climate variability, Clim. Past, 8, 1751–1764, doi:10.5194/cp-8-1751-2012, 2012.

Frisia, S., Borsato, A., Preto, N., and McDermott, F.: Late Holocene annual growth in three Alpine stalagmites records the influence of solar activity and the North Atlantic Oscillation on winter climate, Earth Planet. Sc. Lett., 216, 411–424, 2003.

Genty, D. and Quinif, Y.: Annually laminated sequences in the internal structure of some Belgian stalagmites – Importance for paleoclimatology, J. Sediment. Res., 66, 275–288, 1996.

Genty, D., Baker, A., and Vokal, B.: Intra- and inter-annual growth rate of modern stalagmites, Chem. Geol., 176, 191–212, 2001.

Genty, D., Blamart, D., Ouahdi, R., Gilmour, M., Baker, A., Jouzel, J., and Van-Exter, S.: Precise dating of Dansgaard-Oeschger climate oscillations in western Europe from stalagmite data, Nature, 421, 833–837, 2003.

Kottek, M., Grieser, J., Beck, C., Rudolf, B., and Rubel, F.: World map of the Koppen-Geiger climate classification updated, Meteorol. Z., 15, 259–263, 2006.

Lassen, K. and Friischristensen, E.: Variability of Solar-Cycle length during the past 5 centuries and the apparent association with terrestrial climate, J. Atmos. Terr. Phys., 57, 835–845, 1995.

Le Roy Ladurie, E.: Histoire humaine et comparée du climatôme 1: Canucules et Glaciers XIII et XVIII sciècles, éditions Fayard, 2004.

Luterbacher, J., Xoplaki, E., Dietrich, D., Jones, P. D., Davies, T. D., Portis, D., Gonzalez-Rouco, J. F., von Storch, H., Gyalistras, D., Casty, C., and Wanner, H.: Extending North Atlantic Oscillation reconstructions back to 1500, Atmos. Sci. Lett., 2, 114–124, 2001.

Luterbacher, J., Dietrich, D., Xoplaki, E., Grosjean, M., and Wanner, H.: European seasonal and annual temperature variability, trends, and extremes since 1500, Science, 303, 1499–1503, 2004.

Mangini, A., Spötl, C., and Verdes, P.: Reconstruction of temperature in the Central Alps during the past 2000 yr from a delta O-18 stalagmite record, Earth Planet. Sc. Lett., 235, 741–751, 2005.

Mann, M. E.: The Earth system: physical and chamical dimensions of global environmental change, in: Encyclopedia of Global Environmental Change, edited by: MacCracken, M. C. and Perry, J. S., John Wiley & Sons, Chichester, 504–509, 2002.

Mattey, D., Lowry, D., Duffet, J., Fisher, R., Hodge, E., and Frisia, S.: A 53 year seasonally resolved oxygen and carbon isotope record from a modern Gibraltar speleothem: Reconstructed drip water and relationship to local precipitation, Earth Planet. Sc. Lett., 269, 80–95, 2008.

McDermott, F.: Centennial-scale Holocene climate variability revealed by a high-resolution speleothem delta O-18 record from SW Ireland (9 Nov, pg 1328, 2001), Science, 309, 1816–1816, 2005.

McDermott, F., Atkinson, T. C., Fairchild, I. J., Baldini, L. M., and Mattey, D. P.: A first evaluation of the spatial gradients in delta O-18 recorded by European Holocene speleothems, Global Planet. Change, 79, 275–287, 2011.

Mühlinghaus, C., Scholz, D., and Mangini, A.: Modelling stalagmite growth and delta C-13 as a function of drip interval and temperature, Geochim. Cosmochim. Ac., 71, 2780–2790, 2007.

Mühlinghaus, C., Scholz, D., and Mangini, A.: Modelling fractionation of stable isotopes in stalagmites, Geochim. Cosmochim. Ac., 73, doi:10.1016/j.gca.2009.09.010, 7275–7289, 2009.

Nicholas, F. J. and Glasspoole, J.: General monthly rainfall over England and Wales, 1727 to 1931, British Rainfall, 299–306, 1931.

Niggemann, S., Mangini, A., Mudelsee, M., Richter, D. K., and Wurth, G.: Sub-Milankovitch climatic cycles in Holocene stalagmites from Sauerland, Germany, Earth Planet. Sc. Lett., 216, 539–547, 2003.

Perette, Y.: Etude de la structure interne des stalagmites: contribution a la connaisance geographique des evolutions environnementales du Vercors (France), Unpublished PhD thesis, Geographie, Univ. de Savoie, France, 277 pp., 2000.

Quinif, Y.: Une nouvelle topographie de la Grotte de Han, Lapiaz hors serie "Special Han", 15–18, 1988.

Schmidt, G. A., LeGrande, A. N., and Hoffmann, G.: Water isotope expressions of intrinsic and forced variability in a coupled ocean-atmosphere model, J. Geophys. Res.-Atmos., 112, doi:10.1029/2006JD007781, 2007.

Scholz, D. and Hoffmann, D. L.: StalAge – An algorithm designed for construction of speleothem age models, Quat. Geochronol., 6, 369–382, 2011.

Scholz, D., Muehlinghaus, C., and Mangini, A.: Modelling delta C-13 and delta O-18 in the solution layer on stalagmite surfaces, Geochim. Cosmochim. Ac., 73, 2592–2602, 2009.

Scholz, D., Frisia, S., Borsato, A., Spötl, C., Fohlmeister, J., Mudelsee, M., Miorandi, R., and Mangini, A.: Holocene climate variability in north-eastern Italy: potential influence of the NAO and solar activity recorded by speleothem data, Clim. Past, 8, 1367–1383, doi:10.5194/cp-8-1367-2012, 2012.

Spötl, C. and Mangini, A.: Stalagmite from the Austrian Alps reveals Dansgaard-Oeschger events during isotope stage 3: Implications for the absolute chronology of Greenland ice cores, Earth Planet. Sc. Lett., 203, 507–518, 2002.

Trouet, V., Esper, J., Graham, N. E., Baker, A., Scourse, J. D., and Frank, D. C.: Persistent Positive North Atlantic Oscillation Mode Dominated the Medieval Climate Anomaly, Science, 324, 78–80, 2009.

Van Engelen, A. F. V., Buisman, J., and Ijnsen, F.: A millennium of weather, winds and water in the Low Countries, in: History and Climate, memories of the future?, Kluwer Academics, 101–124, 2001.

Van Rampelbergh, M., Verheyden, S., Allan, M, Quinif, Y., Keppens, E., and Claeys, P.: Monitoring of a fast-growing speleothem

site from the Han-sur-Lesse cave, Belgium, indicates equilibrium deposition of the seasonal δ^{18}O and δ^{13}C signals in the calcite, Clim. Past, 10, 1871–1885, doi:10.5194/cp-10-1871-2014, 2014.

Verheyden, S.: Speleothems as palaeoclimatic archives. Isotopic and geochemical study of the cave environment and its Late Quaternary records, Unpubl, PhD Thesis, Vrije Universiteit Brussel, Belgium, 132 pp., 2001.

Verheyden, S., Baele, J.-M., Keppens, E., Genty, D., Cattani, O., Hai, C., Edwards, L., Hucai, Z., Van Strijdonck, M., and Quinif, Y.: The proserpine stalagmite (Han-sur-Lesse cave, Belgium): Preliminary environmental interpretation of the last 1000 years as recorded in a layered speleothem, Geol. Belg., 9, 245–256, 2006.

Verheyden, S., Genty, D., Deflandre, G., Quinif, Y., and Keppens, E.: Monitoring climatological, hydrological and geochemical parameters in the Pere Noel cave (Belgium): implication for the interpretation of speleothem isotopic and geochemical time-series, Int. J. Speleol., 37, 221–234, 2008.

Verheyden, S., Keppens, E., Quinif, Y., Cheng, H. J., and Edwards, L. R.: Late-glacial and Holocene climate reconstruction as inferred from a stalagmite – Grotte du Pere Noel, Han-sur-Lesse, Belgium, Geol. Belg., 17, 83–89, 2014.

Wackerbarth, A., Scholz, D., Fohlmeister, J., and Mangini, A.: Modelling the delta O-18 value of cave drip water and speleothem calcite, Earth Planet. Sc. Lett., 299, 387–397, 2010.